Journal of Microbiology (2024) 62:33–48
https://doi.org/10.1007/s12275-023-00099-5

MICROBIAL PHYSIOLOGY AND BIOCHEMISTRY

Comparative Transcriptomic Analysis of Flagellar-Associated Genes in *Salmonella* Typhimurium and Its *rnc* Mutant

Seungmok Han[1] · Ji-Won Byun[1] · Minho Lee[1,2]

Received: 27 September 2023 / Revised: 28 November 2023 / Accepted: 29 November 2023 / Published online: 5 January 2024

Abstract

Salmonella enterica serovar Typhimurium (*S*. Typhimurium) is a globally recognized foodborne pathogen that affects both animals and humans. Endoribonucleases mediate RNA processing and degradation in the adaptation of bacteria to environmental changes and have been linked to the pathogenicity of *S*. Typhimurium. Not much is known about the specific regulatory mechanisms of these enzymes in *S*. Typhimurium, particularly in the context of environmental adaptation. Thus, this study carried out a comparative transcriptomic analysis of wild-type *S*. Typhimurium SL1344 and its mutant (Δ*rnc*), which lacks the *rnc* gene encoding RNase III, thereby elucidating the detailed regulatory characteristics that can be attributed to the *rnc* gene. Global gene expression analysis revealed that the Δ*rnc* strain exhibited 410 upregulated and 301 downregulated genes (fold-change > 1.5 and $p < 0.05$), as compared to the wild-type strain. Subsequent bioinformatics analysis indicated that these differentially expressed genes are involved in various physiological functions, in both the wild-type and Δ*rnc* strains. This study provides evidence for the critical role of RNase III as a general positive regulator of flagellar-associated genes and its involvement in the pathogenicity of *S*. Typhimurium.

Keywords *Salmonella* Typhimurium · RNase III · Comparative transcriptomic analysis · Flagellar · Pathogenicity

Introduction

Salmonella poses a substantial public health threat, causing over 300,000 deaths annually, particularly in developing countries (Buckle et al., 2012; Galán, 2021; Majowicz et al., 2010; Moffatt et al., 2016). *Salmonella* is classified into hundreds of serovars based on surface antigenic composition (Brenner et al., 2000; Popoff et al., 2000). Among them, *Salmonella enterica* serovar Typhimurium (*S*. Typhimurium) is an important facultative pathogen that causes food poisoning and gastroenteritis in humans and animals (Galán, 2021; Smith et al., 2016).

The bacterial flagellum, a large filamentous organelle, plays a crucial role in enabling bacterial motility across various environments, including liquids and solid surfaces (Morimoto & Minamino, 2021). *S*. Typhimurium has multiple flagellar on its cell body. The flagellum consists of five distinct structural and functional parts: basal body, hook, junction, filament, and filament cap. Flagellar synthesis and assembly is a highly ordered, hierarchical, and complex process involving more than 200 genes on more than 70 operons (Aldridge & Hughes, 2002; Chevance & Hughes, 2008; Yue et al., 2023). These genes are divided into three classes based on their transcription order (Aldridge & Hughes, 2002; Wang et al., 2022). Class I includes two genes in a single operon, *flhDC*, which are transcribed early in the process and encode important regulatory proteins, FlhD and FlhC (Kutsukake et al., 1990; Yanagihara et al., 1999). Four FlhD and two FlhC proteins assemble into the $FlhD_4C_2$ complex, which functions as a transcription factor for Class II genes (Tomoyasu et al., 2003; Wang et al., 2006). The products of Class II genes form the basal flagellar structure and hook-basal body complex, while Class III genes encode proteins required for filament formation, flagellar rotation (motility), and chemotaxis (Chilcott & Hughes, 2000; Ide et al., 1999; Karlinsey et al., 2000; Minamino et al., 2021; Tomoyasu et al., 2003). The presence of flagellar is also closely associated with the pathogenicity of *S*. Typhimurium

✉ Minho Lee
mlee@hallym.ac.kr

[1] Department of Microbiology, College of Medicine, Hallym University, Chuncheon 24252, Republic of Korea

[2] Institute of Medical Science, College of Medicine, Hallym University, Chuncheon 24252, Republic of Korea

(Lee et al., 2022; Miao et al., 2010; Stecher et al., 2004, 2007; Stewart et al., 2011). Upon entry into the intestinal tract, *S*. Typhimurium utilizes its flagellum to navigate viscous fluids, facilitating attachment to host cells. This strategy enhances infection efficiency and colonization. The flagellum then becomes a major target antigen for the host immune system (Minamino et al., 2021; Wang et al., 2022).

Ribonucleases (RNases) are enzymes that regulate the processing and degradation of target mRNAs and *trans*-acting small non-coding RNAs (Bechhofer & Deutscher, 2019; Deutscher, 2021; Mohanty & Kushner, 2018). Recent studies have shown that RNase-mediated regulation is more widespread than previously thought. For instance, RNase III is an endoribonuclease with specific activity for double-stranded RNA, which acts as a homodimer while playing a key role in the maturation of ribosomal RNAs (rRNAs) and transfer RNAs. In addition, it participates in RNA biogenesis to regulate gene expression (Gordon et al., 2017; Lee et al., 2021a; Lim et al., 2015; Matsunaga et al., 1996; Svensson & Sharma, 2021). Due to its specificity for double-stranded RNA, RNase III has also been implicated in the processing of antisense RNAs and their targets (Lee et al., 2019; Thomason et al., 2015). Furthermore, there are many reports that indicate the involvement of RNase III in the pathogenicity of pathogenic bacteria. For example, RNase III affects the virulence of *Staphylococcus aureus* by cleaving the RNAIII transcript (Boisset et al., 2007; Huntzinger et al., 2005). *S*. Typhimurium expressing a mutant form of RNase III has been shown to exhibit attenuated virulence, impaired motility, and reduced replication in *Galleria mellonella* and mice (Viegas et al., 2013). A recent study also demonstrated that RNase III indirectly affects the expression of *S*. Typhimurium pathogenicity island-1 under anaerobic conditions (Lee et al., 2021c). Transcriptional repression of the *rnc* gene, mediated by the FNR pathway (active under aerobic conditions), enables increased expression of RNase G. This, in turn, accelerates *hns* mRNA degradation, thereby downregulating *hns* mRNA levels in *S*. Typhimurium (Lee et al., 2021c). Despite wide research on the roles of endoribonucleases in bacterial adaptation and pathogenicity, there is a lack of knowledge on the specific regulatory mechanisms of these enzymes in *S*. Typhimurium, particularly in the context of environmental adaptation.

This study explored RNase III-regulated properties through comparative global gene expression analyses and phenotypic tests, including motility, biofilm formation, and host cell invasion, in both the *S*. Typhimurium SL1344 wild-type (WT) and Δ*rnc* strains, revealing RNase III as a general positive regulator of flagellar-associated genes that coordinates a comprehensive genetic and physiological regulatory process necessary for pathogenicity in *S*. Typhimurium.

Materials and Methods

Animals

Mouse feeding and experimental procedures were performed as described previously (Lee et al., 2021c; Song et al., 2019). Nara Biotech supplied the specific pathogen-free 4-week-old female BALB/c mice ($n = 34$) used in the study.

Bacterial Strains and Plasmid Construction

S. Typhimurium and *Escherichia coli* strains were cultured at 37 °C in Luria–Bertani (LB) medium (BD Biosciences) containing specific antibiotics (100 μg/ml ampicillin and/or 5 μg/ml tetracycline; Sigma-Aldrich).

Tables 1 and 2 contain details about the bacterial strains, plasmids, and primers used in this study. The Δ*rnc* strain was constructed as described previously (Lee et al., 2021c).

Briefly, pSt-rnc was constructed by amplifying the coding region of *S*. Typhimurium *rnc*, which then digested with XhoI and BamHI and ligated into pACYC177. To construct the pET-Ecrnc plasmid expressing *E. coli* RNase III, NdeI and XhoI sites were generated using PCR methods. The PCR products were digested with NdeI and XhoI and then cloned into pET-22b(+) (Novagen).

Cell Lines and Culture Conditions

Human colorectal intestinal epithelial carcinoma cells (HCT116) were cultured in McCoy's 5A medium (ATCC), supplemented with 10% (v/v) heat-inactivated fetal bovine serum (Avantor) and 1% (v/v) penicillin–streptomycin solution (Gibco). The cell lines were cultured at 37 °C, in a humidified atmosphere containing 5% CO_2.

Purification of *E. coli* RNase III

The purification of His-tagged *E. coli* RNase III was performed as described previously (Sim et al., 2010).

Preparation of RNase III Protein and CpG-DNA Co-Encapsulated in Liposome Complexes

Sigma-Aldrich supplied the liposomes 1, 2-dioleoyl-*sn*-glycero-3-phosphoethanolamine (DOPE) and cholesteryl hemisuccinate (CHEMS). Briefly, DOPE and CHEMS were mixed in ethanol at a molar ratio of 1:1. The mixture was evaporated with nitrogen gas to produce a solvent-free lipid film, which was then resuspended in a mixture containing equal volumes of water-soluble CpG-DNA and RNase III protein. The CpG-DNA comprises 20 bases containing

Table 1 Bacterial strains and plasmids used in this study

Strains or plasmids	Relevant characteristics	References
S. Typhimurium		
SL1344	*hisG46*, *rpsL*, Str^R	Hoiseth and Stocker (1981)
Δ*rnc*	Same as SL1344, but *rnc-14*::Tn*10*, Tc^R	Lee et al., (2021c)
E. coli		
DH5α	F^-, φ80d*lacZ*ΔM15, Δ(*lacZYA-argF*)U169, *rec*A1, *end*A1, *hsd*R17($r_K^-m_K^+$), *pho*A, *sup*E44, λ^-, *thi*-1, *gyr*A96, *rel*A1	Laboratory strain
BL21(DE3)	F^-, *omp*T, *hsd*S_B(r_B^-, m_B^-), *gal*, *dcm*, (DE3)	Thermo Fisher Scientific
Plasmids[a]		
pACYC177	p15A *ori*, Amp^R, Km^R	Chang and Cohen (1978)
pSt-rnc	pACYC177 containing the *S*. Typhimurium *rnc* gene, Amp^R	This study
pET22b(+)	ColE1 *ori*, *bla*, *lac*I, T7p, Cloning vector with His tag, Amp^R	Novagen
pET-Ecrnc	pET22b(+) containing the *E. coli rnc* gene with His tag, Amp^R	This study

[a]See Materials and Methods for a detailed plasmid description scheme

Abbreviation: Amp^R, ampicillin resistance; Km^R, kanamycin resistance; Tc^R, tetracycline resistance; Str^R, streptomycin resistance

Table 2 Primers used in this study

Primers	Sequences (5′–3′)
Construction of pSt-rnc	
St-rnc F (XhoI)	ATCTCGAGAAATTCCCTAAGACTAACGA
St-rnc R (BamHI)	AACGGATCCGTCATTCCAACTCCAGTTTTT
Construction of pET-Ecrnc	
Ecrnc F (NdeI)	TTCATATGAACCCCATCGTAATTAATCG
Ecrnc R (XhoI)	AACTCGAGTTCCAGCTCCAGTTTTTTCA
For qRT-PCR	
RT-gdh-F	TTCCTACTCTGGCCTCAACG
RT-gdh-R	TTCCGCTTCAAACCAGGTTG
RT-rng-F	ACCGTAATCTCGACGACACC
RT-rng-R	GCGGCGATGATCTTCATTAT
RT-ydiV-F	CAGCAGCGAGCTGAAATGAT
RT-ydiV-R	CGCAAACATCGCCTCAGTAT
RT-pnp-F	TACCGCATCACCGATAAACA
RT-pnp-R	ATGTCTTTTTCACGGCCATC
RT-flhD-F	CGCCTCGGTATCAACGAAGA
RT-flhD-R	CTCCGCCAGTTTGACCATCT
RT-fliA-F	CTTACCCAGTTTGGTGCGTA
RT-fliA-R	CGAGCAACTGGTGTTAACGC
RT-fliC-F	CGCAGTAAAGAGAGGACGTT
RT-fliC-R	GGGCAACACCGTAAACAACC
RT-flgE-F	CGGACCCTGTACCGTCTAAA
RT-flgE-R	AAGGAAGCTGAGGGAGAAGG
RT-cheZ-F	GATCTGACGGGTCAGGTGAT
RT-cheZ-R	ACCTGATCCTGACTGGCAAC
RT-tsr-F	ATGGGCAACAACGATCTCTC
RT-tsr-R	CTGTCTCTGACGCACTCAGC
RT-flgH-F	AGTAAAAGCTCGTCGGCAAA
RT-flgH-R	AAAGGTATTGCTGGCATTCG

three CpG motifs (underlined; 5′-AGCAGCGTTCGTGT CGGCCT-3′). The resuspended mixture underwent vigorous stirring for 30 min, at 25 °C. After adjustment of pH to a level of 7.0, the lipoplex solution was sonicated for 30 s, filtered through a 0.22-μm filter, and subjected to three freeze–thaw cycles with liquid nitrogen (Kim et al., 2011, 2015).

Mice and Immunization

The mice were maintained under specific pathogen-free conditions and intraperitoneally injected with RNase III protein (50 μg) and CpG-DNA (50 μg) co-encapsulated in a DOPE:CHEMS complex, three times, at 10 day intervals (Kim et al., 2011, 2015).

Production of Mouse Anti-RNase III Monoclonal Antibody

Splenocytes obtained from RNase III-immunized mice were fused with mouse myeloma cells (SP2/0) using a polyethylene glycol solution (Sigma-Aldrich). The hybridoma clones were selected in hypoxanthine-aminopterine-thymidine and hypoxanthine-thymidine media (both from Sigma-Aldrich), following the standard hybridoma production protocol (Yokoyama et al., 2006). The selected hybridoma cells were injected into mice to produce ascites fluid. The anti-RNase III monoclonal antibody was purified from the ascites fluid using protein A column chromatography (Bio-Rad Laboratories) (Kim et al., 2011, 2015).

Western Blot Analysis

Proteins were separated and analyzed using western blot, as described previously (Lee et al., 2021c). GAPDH was used as a loading control.

Growth Curve

Pre-cultured *S*. Typhimurium strains (WT, Δ*rnc*, and Δ*rnc*-^{comp}) were diluted in LB medium containing ampicillin (100 μg/ml) and incubated at 37 °C for 10 h, in a shaking incubator maintained at 240 rpm. The growth rate of *S*. Typhimurium was monitored by measuring the cell density [in terms of the optical density at the wavelength of 600 nm (OD_{600})] at the indicated time-points. The experiments were conducted in triplicate.

RNA Isolation

S. Typhimurium SL1344 WT and Δ*rnc* strains containing pACYC177 were grown at 37 °C in LB medium supplemented with ampicillin (100 μg/ml). The cultured cells were then diluted 1:100 in the same fresh medium and incubated at 37 °C until they reached an OD_{600} of 1.0. Total RNA was isolated using an RNeasy Mini Kit (Qiagen), following the manufacturer's instructions. RNA quality was assessed on an Agilent 2100 Bioanalyzer using the RNA 6000 Nano Chip (Agilent Technologies), and RNA quantification was performed on an ND-2000 spectrophotometer (Thermo Fisher Scientific).

Library Preparation and RNA-Sequencing (RNA-seq)

For the control and test RNAs, rRNA was depleted from 1 μg of total RNA using the RiboCop rRNA Depletion for Bacteria Probe Mix G ± Kit (Lexogen). Following the manufacturer's instructions, the NEBNext Ultra II Directional RNA-seq Kit (New England BioLabs) was used for library construction, and the rRNA-depleted RNAs were used for cDNA synthesis and shearing. Illumina indexes 1–12 were used for indexing, followed by PCR enrichment. Libraries were screened for average fragment size using the TapeStation HS D1000 Screen Tape (Agilent Technologies) and a library quantification kit on a StepOne Real-Time PCR System (Life Technologies). High-throughput sequencing was performed as paired-end 100 sequencing on NovaSeq 6000 System (Illumina).

Data Analysis

To generate the alignment file, paired-end RNA-seq reads were aligned to the *S*. Typhimurium SL1344 genomic DNA reference (GCF_000210855.2 ASM21085v2) from the National Center for Biotechnology Information database, using the Bowtie2 software tool. Differentially expressed genes (DEGs) were determined based on counts from unique and multiple alignments, using the EdgeR package (Gentleman et al., 2004) within R. The screening criteria included genes with raw p values < 0.05 and fold-change > 1.5 (Na, 2020). The alignment file was also used for transcript assembly. The trimmed mean of the M-values and counts per million mapped reads normalization methods were applied to the raw read counts. Following that, the p values for comparisons between samples were calculated using the Student's t-test and analysis of variance.

Gene Ontology (GO) and Kyoto Encyclopedia of Genes and Genomes (KEGG) Enrichment Analysis of DEGs

The KEGG database was used to obtain a database of metabolic pathways, regulons, and genomic islands of related

species (Kanehisa & Goto, 2000). GO terms were obtained from the UniProt database (The UniProt Consortium, 2018) through a programmatic query. We utilized these functional annotation data for enrichment analysis, to enhance our comprehension of the functions and metabolic pathways associated with the DEGs. Fisher's exact probability test was used as a statistical method to determine the relationship between a gene set and pathways or GO terms. Pathways and GO terms that were significant ($p < 0.05$) have been displayed in graphs. The protein network was generated using the STRING version 11.0 web tool (https://string-db.org) (Szklarczyk et al., 2019).

Confirmation of DEGs Using Quantitative Reverse Transcription PCR (qRT-PCR)

The RNA-seq data were validated by means of qRT-PCR analysis of select genes. Total cellular RNA extraction was performed as described above and qRT-PCR was performed as described previously (Lee et al., 2021c).

Measurement of Motility Capacity

To evaluate the swimming and swarming motilities, *S*. Typhimurium strains were initially incubated overnight on LB agar, at 37 °C. Subsequently, a single colony from the agar surface was inoculated onto 0.3% LB agar (for swimming motility) or 0.5% LB agar containing 0.5% glucose (for swarming motility) and the inoculated plates were then incubated for 9 h at 37 °C. The distances from the inoculation zone on the agar plates to the edge of the swimming and swarming zones were measured using ImageJ software (National Institutes of Health). This experiment was conducted in five parallel runs and three replicates each (Has et al., 2023; Lee et al., 2021b, 2022).

Quantification of Biofilm Formation

Biofilm formation was measured by assessing the adherence of *S*. Typhimurium strains (WT, Δ*rnc*, and Δrnc^{comp}) to borosilicate tube wells, as described previously (Has et al., 2023; Lee et al., 2021b).

Measurement of Flagellar Number and Length

To investigate the impact of RNase III expression on flagellar number and length, the strains utilized in the motility assay underwent further analysis by means of transmission electron microscopy. Cells were grown at 37 °C in LB medium until they reached an OD_{600} of 1.0. The cultures were diluted with triple distilled water and transferred onto Formvar film, followed by negative staining with 1% phosphotungstic acid. Samples were observed using a JEM-2100F transmission electron microscope (JEOL). Flagellar length was determined using ImageJ software.

Cell Infection Assay

The cell infection assay was performed as described previously (Lee et al., 2021c).

Trypan Blue Exclusion Assay

HCT116 cells were seeded at a density of 1×10^4 cells/well and incubated for 24 h in an incubator containing 5% CO_2, at 37 °C. Before starting the experiment, antibiotic-containing McCoy's 5A medium was replaced with antibiotic-free McCoy's 5A medium. HCT116 cells were infected with *S*. Typhimurium strains at a multiplicity of infection of 100 and incubated for 1, 2, 3, and 4 h. Following that, the cells were washed with serum-free McCoy's 5A medium containing gentamicin (100 μg/ml) and phosphate-buffered saline. After trypsin-ethylenediaminetetraacetic acid-mediated cell harvesting, viable and dead cells were counted using trypan blue staining. The percentage of viable cells was calculated as follows: viable cells (%) = (total number of viable cells/ml of aliquot / total number of cells/ml of aliquot) × 100.

Quantification and Statistical Analysis

Statistical details for all experiments are provided in the figure legends. Multiple comparisons were performed using the Student–Newman–Keuls test, in SAS version 9.2 (SAS Institute), while control comparisons were conducted using Student's *t*-tests in both SAS version 9.2 and SigmaPlot 10.0 (Systat Software). Data are presented as mean ± standard error of the mean, with a *p*-value of < 0.05 indicating statistical significance.

Results

RNase III Expression Affects the mRNA Abundance of a Subset of Genes in *S.* Typhimurium

RNase III, a member of the double-stranded RNA-specific endoribonuclease family, is present in essentially all bacteria and plays numerous roles in RNA metabolism (Bechhofer & Deutscher, 2019; Deutscher, 2021; Lim et al., 2015; Mohanty & Kushner, 2018). Furthermore, we found homologues of RNase III in closely related Enterobacteriaceae (Fig. S1). Among them, RNase III of *S*. Typhimurium was found to be highly homologous to that of *E. coli*, with a 98.67% amino acid sequence identity (Fig. 1A).

We first investigated whether RNase III levels affect *S*. Typhimurium growth. To evaluate this, the

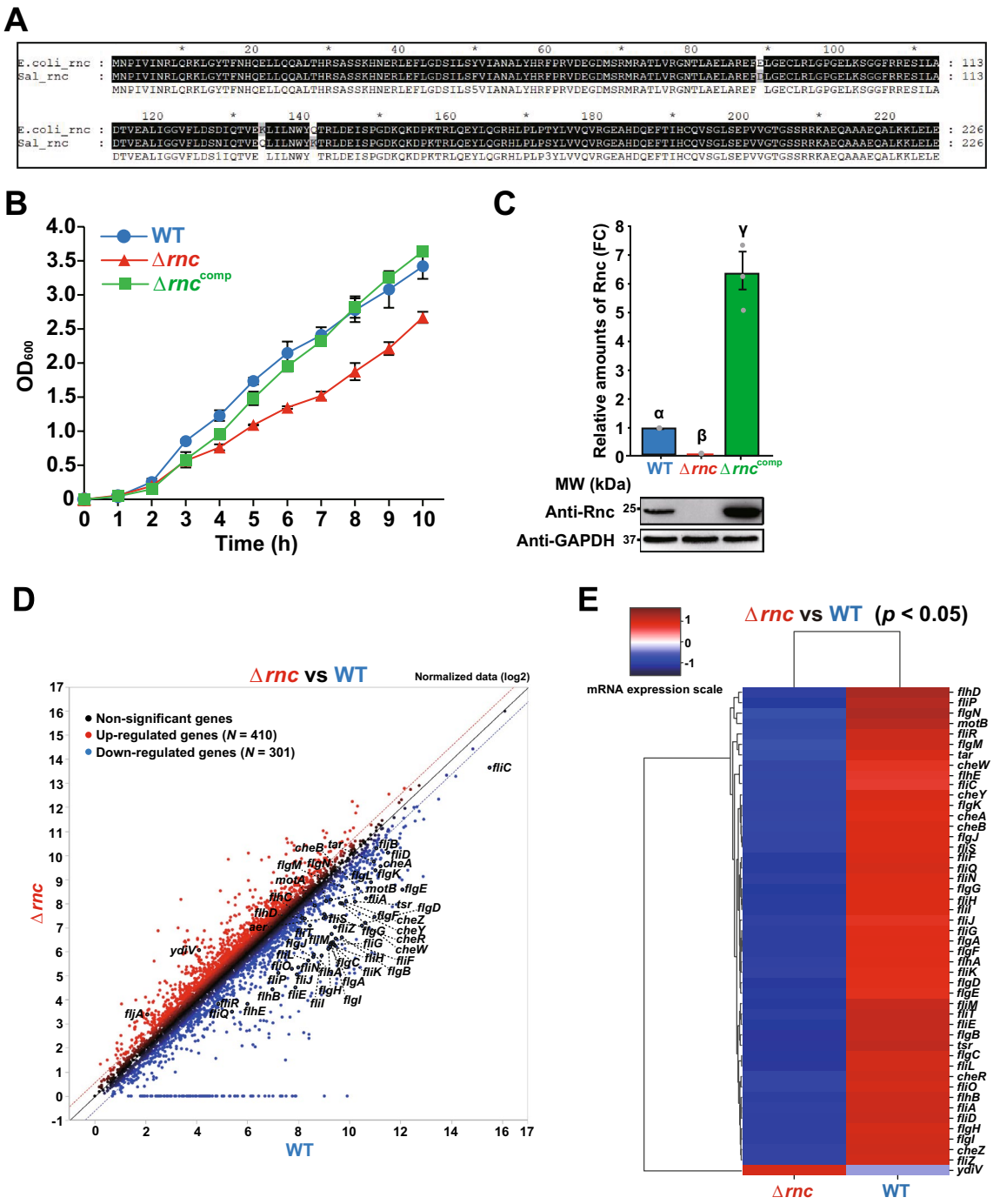

cell densities of three *S.* Typhimurium strains, wild-type (WT; SL1344 + pACYC177), *rnc*-deleted (Δ*rnc*; SL1344*rnc* + pACYC177), and *rnc*-complemented (Δ*rnc*^{comp}; SL1344*rnc* + pSt-rnc), were monitored at different time-points (h). The Δ*rnc* strain exhibited a lower growth rate than the WT strain. However, the growth rate was restored to that of the WT strain upon complementation with the *rnc* gene (Δ*rnc*^{comp}; Fig. 1B). This phenomenon has been previously observed as well for RNase III expression, using the slow-growing phenotype of *E. coli* cells lacking the *rnc* gene (Sim et al., 2010). Western blot analysis revealed that the Δ*rnc*^{comp} cells displayed ~ 6.4-fold higher RNase III protein levels than the WT strain (Fig. 1C). However, the increased expression levels of RNase III did not affect the growth rates of the Δ*rnc*^{comp} strain (Fig. 1B, C).

To investigate the potential impact of RNase III expression on mRNA levels, total RNAs extracted from both the WT and Δ*rnc* strains were subjected to RNA-seq analysis.

◂**Fig. 1** Analysis of DEGs in the WT and Δ*rnc* strains. **A** Amino acid sequence alignment of *E. coli* RNase III (E. coli_rnc) and *S.* Typhimurium RNase III (Sal_rnc). Amino acid sequences of *E. coli* and *S.* Typhimurium RNase III were obtained from the National Center for Biotechnology Information database (AAA79829.1 and AAL21475.1, respectively). The sequences were aligned using ClustalW (https://www.genome.jp/tools-bin/clustalw) and visualized using GeneDoc software. Black backgrounds represent identical residues, while white or gray backgrounds indicate dissimilar residues. Numbers below the sequence alignment represent amino acid sequence similarity scores. **B** Growth rates of the WT, Δ*rnc*, and Δ*rnc*^{comp} strains. *S.* Typhimurium cells were grown at 37 °C in LB medium supplemented with ampicillin (100 μg/ml). Growth was monitored by measuring the OD_{600} at the indicated time-points. The experiments were conducted in triplicate. **C** Western blot analysis of RNase III in *S.* Typhimurium strains (WT, Δ*rnc*, and Δ*rnc*^{comp}). WT RNase III levels were set to 1, and GAPDH was used as an internal standard. Western blot data were analyzed using one-way analysis of variance with Student–Newman–Keuls test ($p < 0.0001$). Data represent mean ± s.e.m. of at least three independent experiments. Statistically significant differences have been indicated using distinct Greek letters. **D** Scatter plots of the DEGs. Genes in red and blue met the criteria of $|\log_2 FC| > 0.5$ and p-value < 0.05. Genes shown in black were identified as non-significant, because they did not meet the criteria mentioned above. **E** Heatmap of flagellar-associated mRNAs showing significant differences in expression ($p < 0.05$) between the *S.* Typhimurium WT and Δ*rnc* strains. On the mRNA expression scale, red indicates higher mRNA expression, while blue indicates lower mRNA expression. DEGs, differentially expressed genes; FC, fold-change

DEG analysis was performed using four methods: scatter plots, heatmaps, GO enrichment analysis, and KEGG pathway enrichment analysis. Scatter plots were used to display the overall distribution of DEGs in the WT and Δ*rnc* strains. Fold-change > 1.5 and $p < 0.05$ were used as selection criteria for the DEGs. This study identified 711 significant DEGs (301 downregulated and 410 upregulated) in the experimental group (Fig. 1D).

We employed a heatmap and hierarchical clustering method to determine the expression patterns of different genes. As genes with same or similar expression patterns may have similar functions or be involved in the same metabolic process or cellular pathway, these were clustered into classes, to predict the function of unknown genes or discover new functions of known genes. Although the Δ*rnc* strain exhibited significantly increased mRNA levels of the flagellar negative regulator gene *ydiV*, it demonstrated significantly decreased mRNA levels of 46 flagellar-associated genes (including flagellar structural, motor, and chemotaxis proteins) (Fig. 1D, E). Table 3 presents the 47 flagellar-associated genes that were found to be altered by RNase III expression. Overall, these results suggested that RNase III may contribute to the mRNA abundance of a subset of genes within the *S.* Typhimurium transcriptome.

RNase III Contributes to the Stabilization of Numerous mRNAs in the *S.* Typhimurium Transcriptome

GO is a classification system for molecular functions, biological processes, and cellular components. Figure 2 represents the results of the GO enrichment analysis of the DEGs, which was used to investigate the variances in cellular components, biological processes, and molecular functions between the Δ*rnc* and WT strains. The Δ*rnc* strain was enriched in terms associated with flagellar assembly-related cellular components, as well as large and small ribosomal subunits (Fig. 2A).

The biological process classification results of the GO analysis revealed enrichment of DEGs distributed across various categories, including flagellar assembly, cell motility (swimming and swarming), chemotaxis, organelle assembly, and peptide metabolic process (Fig. 2B), while the molecular function classification results revealed enrichment of DEGs involved in cytoskeletal motor activity, structural constituent of ribosome, rRNA binding, structural molecular activity, protein binding, RNA binding, and catalytic activity (Fig. 2C).

Collectively, these experimental data suggested that RNase III may contribute to stabilizing numerous mRNAs within the *S.* Typhimurium transcriptome while revealing a strong association between RNase III and flagellar assembly.

RNase III Levels Affect the Expression of Flagellar-Associated Genes in *S.* Typhimurium

Comparative transcriptomic analysis revealed lower expression levels of flagellar assembly-associated genes in the Δ*rnc* strain than in the WT strain (Figs. 1D, E, 2). Given the direct effect of the flagellum on bacterial pathogenicity, affecting motility, biofilm formation, adherence, host cell invasion, and secretion of virulence factors (Haiko & Westerlund-Wikstrom, 2013), we hypothesized that RNase III is involved in regulating flagellar assembly.

To investigate the relationship between genes involved in flagellar assembly, we performed an analysis using STRING program, which determines the relationships between DEGs. The analysis revealed an association between the genes involved in flagellar assembly and chemotaxis (Fig. 3A).

To further validate the gene expression profiling, qRT-PCR was conducted on 10 selected genes, comprising of 3 upregulated and 7 downregulated genes (Fig. 3B). Consistent with the results of the RNA-seq, the expression of flagellar-associated genes (*flhD*, *fliA*, *fliC*, *flgE*, *cheZ*, *tsr*, and *flgH*) was downregulated in the Δ*rnc* strain, with a high coefficient of determination ($R^2 = 0.9223$) (Fig. 3B, C), thereby validating the reliability of the RNA-seq data in identifying DEGs for subsequent analysis.

Table 3 Relative expression levels of flagellar-associated genes in the Δ*rnc* strain

Genes	Function	Fold change (Δ*rnc*/WT)	*p* value
ydiV	Negative regulator of FlhDC expression	3.943	0.02261
flhD	Master regulator for flagellar genes	0.618	0.03460
flgN	Export chaperone specific for FlgK and FlgL	0.514	0.04029
flgM	Anti-sigma factor	0.505	0.00981
fliR	Type III export gate protein	0.484	0.00194
motB	Stator, transmembrane proton channel	0.474	0.01698
tar	Methyl-accepting chemotaxis protein	0.430	0.00533
fliT	Export chaperone specific for FliD	0.392	0.00530
fliD	Filament cap	0.379	0.00149
cheR	Chemotaxis protein	0.371	0.00018
flgK	Hook-filament junction	0.325	0.00579
cheW	Chemotaxis protein	0.325	0.02211
fliS	Export chaperone specific for FliC	0.321	0.00381
cheA	Chemotaxis protein	0.315	0.00859
cheY	Chemotaxis protein	0.312	0.00182
cheB	Chemotaxis protein	0.306	0.00329
cheZ	Chemotaxis protein	0.296	0.00010
fliC	Filament (H1 flagellin)	0.278	0.04925
fliQ	Type III export gate protein	0.271	0.00087
fliP	Type III export gate protein	0.237	0.03577
tsr	Methyl-accepting chemotaxis protein	0.229	0.01607
flhE	Plug for a proton channel in a type III export apparatus	0.225	0.04906
fliA	Sigma factor/Chaperone specific for FlgM	0.187	0.00132
fliZ	Positive regulator for flagellar gene expression	0.186	0.00020
fliO	Scaffolding protein for the assembly of the $FliP_5FliR_1$ complex	0.183	0.00033
flhB	Type III export gate protein, protein export switch	0.171	0.00089
fliM	C ring, directional switch	0.170	0.00375
fliL	Stator associated protein	0.161	0.00059
flhA	Type III export gate protein, energy transducer, protein export switch	0.152	0.01476
fliN	C ring, directional switch	0.149	0.00734
flgJ	Rod cap, Muramidase	0.143	0.00644
fliJ	Type III export apparatus, central stalk	0.137	0.04078
fliK	Hook-length control	0.135	0.02433
fliF	MS ring	0.133	0.00347
fliH	Type III export apparatus, peripheral stalk	0.129	0.01090
flgI	P ring	0.128	0.00004
flgA	Periplasmic chaperone for P ring assembly	0.124	0.01793
flgH	L ring	0.121	0.00068
fliG	C ring, torque generation, directional switch	0.121	0.02206
fliI	Type III export apparatus, ATPase	0.118	0.00949
flgB	Proximal rod	0.115	0.01029
flgC	Proximal rod	0.109	0.00025
fliE	Basal body protein connecting the MS ring and the proximal rod	0.096	0.01292
flgG	Distal rod	0.095	0.01322
flgD	Hook cap	0.094	0.02753
flgE	Hook	0.089	0.04133
flgF	Proximal rod	0.087	0.02529

Data represent genes with increased and decreased expression, exhibiting a fold change greater than 1.5 and significant differences (Δ*rnc* strain versus WT strain)

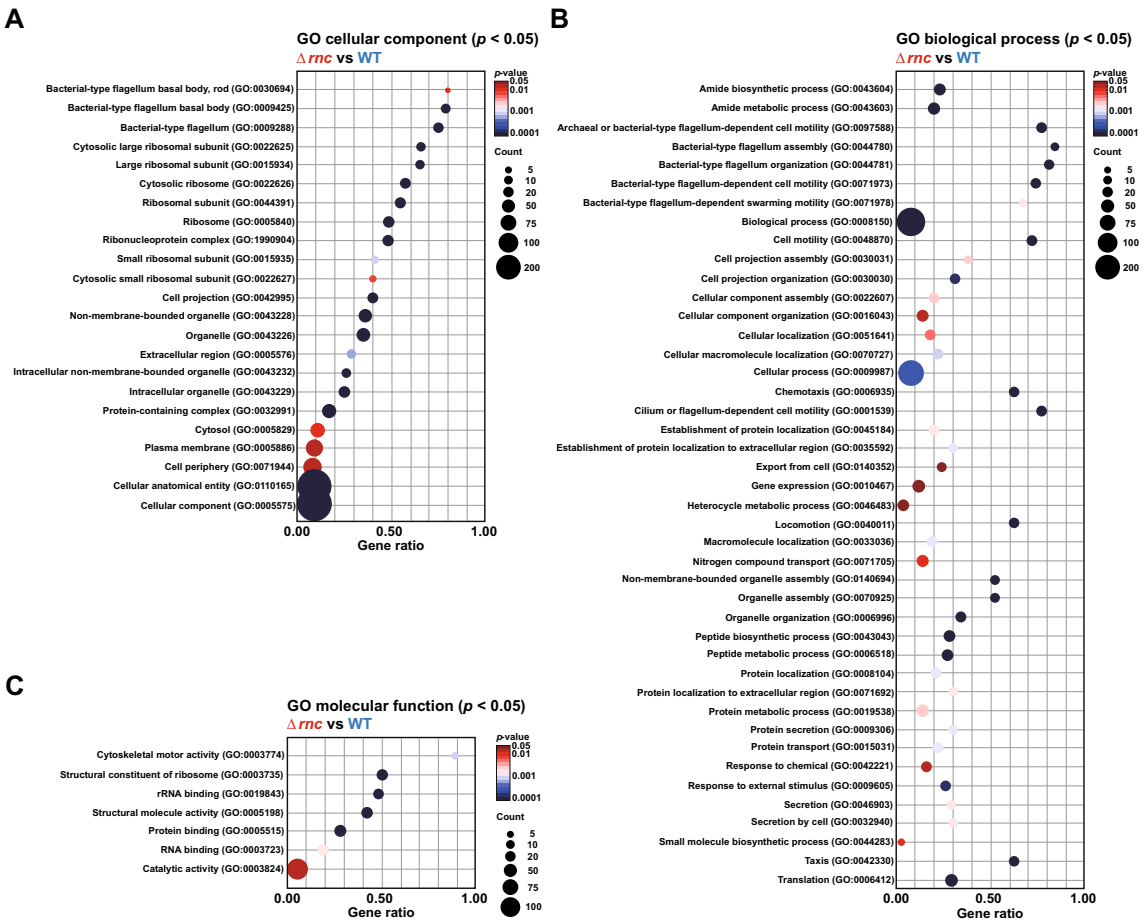

Fig. 2 Classification analysis of DEGs in the WT and Δ*rnc* strains. GO **A** cellular component, **B** biological process, and **C** molecular function analyses of the DEGs. For (**A**), (**B**), and (**C**), the x-axis represents the gene ratio, where was calculated as the number of DEGs enriched in each term divided by the total number of all genes in each term. The y-axis represents significantly enriched GO terms based on the DEGs. The size of the circle is proportional to the number of genes. GO, Gene Ontology; DEGs, differentially expressed genes

RNase III Levels Affect Motility, Biofilm Formation, and Flagellar Synthesis in *S.* Typhimurium

Two methods were used to assess motility to determine whether the downregulated flagellar-associated gene expression was linked to the phenotype. The Δ*rnc* cells showed lower swimming motility (measured on 0.3% LB agar plates) than the WT cells. However, when RNase III was exogenously expressed (Δ*rnc*^{comp} cells), swimming motility was restored (Fig. 4A). Swarming motility was measured on 0.5% LB agar plates containing 0.5% glucose, and the results were consistent with those shown in Fig. 4B.

To further investigate whether motility loss affects biofilm formation, we assessed the biofilm formation of the *S.* Typhimurium strains. The optimal biofilm formation temperature of the *S.* Typhimurium strains used in this study was determined to be 20 °C in a previous study (Has et al., 2023). In this study, the capacity of the strains to form biofilms was determined at 24, 48, 72, 96, 120, 144, and 168 h. The optimum time for biofilm formation was 96 h (Fig. 4C). The degree of biofilm formation decreased by ~ 30% in the Δ*rnc* strain, as compared to that in the WT strain, and was again restored in the Δ*rnc*^{comp} strain (Fig. 4C).

To determine the basis for the above phenotypes, we examined the flagellar synthesis of the *S.* Typhimurium strains using negative staining electron microscopy (Fig. 4D). No or fewer flagellar were observed in the Δ*rnc* strain, as compared to those in the WT and Δ*rnc*^{comp} strains. Additionally, the Δ*rnc* strain displayed ~ 95% reduced flagellar length than the WT strain, while the Δ*rnc*^{comp} strain displayed a length that was restored to the WT strain level (Fig. 4D). Furthermore, we observed a decrease in cell size in the Δ*rnc* strain (Fig. 4D). In Fig. 3B, the Δ*rnc* strain displayed ~ 1.6-fold increased mRNA expression of *rng*. This has been confirmed in previous studies as well, where the expression level of Rng (RNase G) protein was found to be higher in the *E. coli* and *S.* Typhimurium Δ*rnc* strains, as compared to the respective WT strains (Lee et al., 2021c;

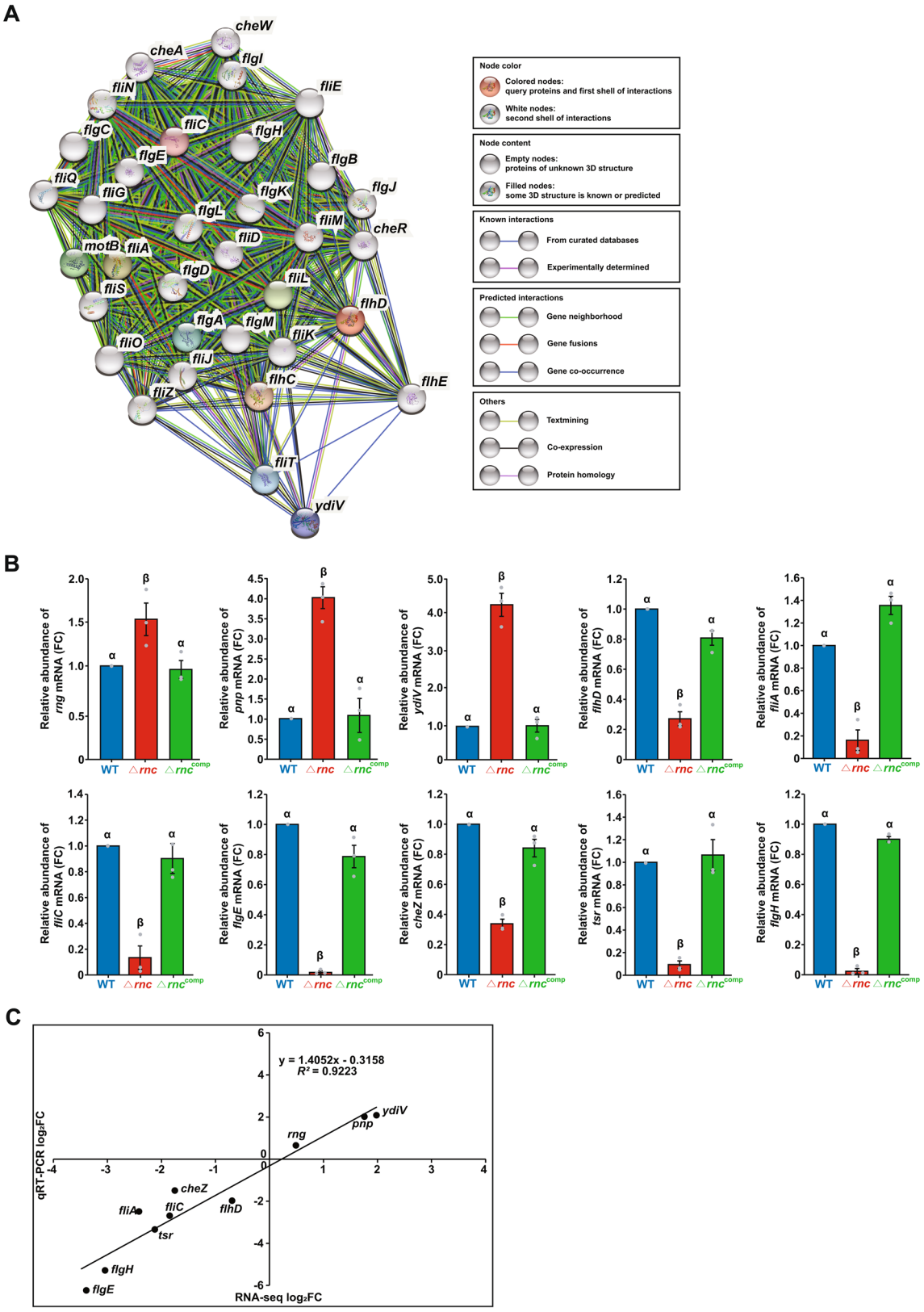
A
cheW
cheA
flgI
fliN
fliE
fliC
flgH
flgC
flgE
flgB
fliQ
fliG
flgK
flgJ
flgL
fliM
cheR
motB
fliA
fliD
flgD
fliL
fliS
flhD
flgA
flgM
fliK
fliO
fliJ
flhC
flhE
fliZ
fliT
ydiV
Node color
Colored nodes: query proteins and first shell of interactions
White nodes: second shell of interactions
Node content
Empty nodes: proteins of unknown 3D structure
Filled nodes: some 3D structure is known or predicted
Known interactions
From curated databases
Experimentally determined
Predicted interactions
Gene neighborhood
Gene fusions
Gene co-occurrence
Others
Textmining
Co-expression
Protein homology
B
Relative abundance of rng mRNA (FC)
Relative abundance of pnp mRNA (FC)
Relative abundance of ydiV mRNA (FC)
Relative abundance of flhD mRNA (FC)
Relative abundance of fliA mRNA (FC)
Relative abundance of fliC mRNA (FC)
Relative abundance of flgE mRNA (FC)
Relative abundance of cheZ mRNA (FC)
Relative abundance of tsr mRNA (FC)
Relative abundance of flgH mRNA (FC)
WT
△rnc
△rnc^comp
C
y = 1.4052x - 0.3158
R² = 0.9223
qRT-PCR log₂FC
RNA-seq log₂FC
ydiV
pnp
rng
cheZ
fliA
fliC
flhD
tsr
flgH
flgE

◂**Fig. 3** Analysis of the mRNA expression of DEGs in *S*. Typhimurium. **A** Interactions of flagellar-associated proteins. The network of proteins encoded by flagellar-associated genes from among the DEGs was drawn using the STRING database (https://string-db.org). **B** Analysis of the mRNA expression of *rng*, *pnp*, and flagellar-associated genes (*ydiV*, *flhD*, *fliA*, *fliC*, *flgE*, *cheZ*, *tsr*, and *flgH*) in *S*. Typhimurium strains (WT, Δ*rnc*, and Δ*rnc*^{comp}), using qRT-PCR. The mRNA expression levels of the DEGs in the WT strain were set to 1. The data were analyzed using one-way analysis of variance with Student–Newman–Keuls test ($p < 0.0001$). The data represent mean ± s.e.m. of at least three independent experiments. Statistically significant differences have been indicated using distinct Greek letters. **C** qRT-PCR validation of the DEGs. The x-axis represents RNA-seq $\log_2$FC, while y-axis represents qRT-PCR $\log_2$FC. For (**B**) and (**C**), the mRNA expression levels of the DEGs were normalized to the expression of *gdh* mRNA. Gene expression was quantified using the $2^{-\Delta\Delta Ct}$ method. DEGs, differentially expressed genes; FC, fold-change

Song et al., 2014). In other studies, overexpression of the *rng* gene did not affect growth, but led to decreased cell size (minicells) or altered cell morphology (chained cells) (Okada et al., 1994; Song et al., 2014). These findings show that deletion of the *rnc* gene leads to overexpression of Rng, which results in decreased cell size.

Overall, these results suggest that RNase III levels impact flagellar synthesis, potentially influencing motility and biofilm formation in *S*. Typhimurium.

RNase III Levels Influence *S*. Typhimurium Pathogenicity

In many pathogenic bacteria, flagellar-mediated motility is closely linked to processes, such as host cell invasion and virulence (Duan et al., 2013; Echazarreta & Klose, 2019; Josenhans & Suerbaum, 2002). Our experimental results showed that RNase III levels affected flagellar synthesis while influencing the motility and biofilm formation of *S*. Typhimurium (Fig. 4). Therefore, we analyzed the effects of RNase III levels on *S*. Typhimurium pathogenicity using various methods. The host invadability of *S*. Typhimurium cells was first tested using a cell infection assay—an excellent system for studying *S*. Typhimurium virulence, because mutants with defective invasion and persistence in host cells exhibit significantly reduced virulence in animal hosts (Lee et al., 2021c, 2022; Pati et al., 2013; Raffatellu et al., 2005). HCT116 was infected with *S*. Typhimurium strains (WT, Δ*rnc*, and Δ*rnc*^{comp}) for 1 h to facilitate invasion and then subjected to gentamicin treatment to eliminate any remaining extracellular bacteria. The number of invading bacteria reduced by 59% in Δ*rnc* cells, as compared to that in the WT cells (Fig. 5A), but was restored to that of the WT cells when the Δ*rnc* cells were complemented with exogenous expression of *rnc* (Δ*rnc*^{comp}) (Fig. 5A). A cytotoxicity assay conducted to evaluate *S*. Typhimurium pathogenicity in vitro revealed that, at all time-points, the *S*. Typhimurium-mediated cytotoxicity at an multiplicity of infection of 100 was lower in the Δ*rnc* cells than in the WT cells, but restored to the WT levels in the Δ*rnc*^{comp} cells (Fig. 5B).

These results suggest an association between RNase III levels and *S*. Typhimurium pathogenicity.

Discussion

The flagellum serves as an important motility organelle that facilitates bacteria movement. The construction of bacterial flagellar involves the synthesis of flagellar proteins, which is a highly energy-consuming process. In the early stages of *Salmonella* infection, flagellar-mediated motility facilitates the gastrointestinal colonization of sites preferred by *Salmonella* (Chaban et al., 2015; Horstmann et al., 2020; Wang et al., 2022). Although many studies have revealed the structure and assembly of the *Salmonella* flagellar complex, the regulation of flagellar synthesis in *Salmonella* under different conditions remains controversial.

Here, we demonstrate that RNase III levels influence several pathogenesis-related processes of *S*. Typhimurium, as well as the expression of flagellar-related genes. Mutations in RNase III (Δ*rnc*) resulted in the differential expression of approximately 700 genes (fold-change > 1.5 and $p < 0.05$), which represent ~ 20% of the *S*. Typhimurium genome. Figures 1 and 2 show that numerous transcripts are differentially expressed in the Δ*rnc* strain, as compared to those in the WT strain. With respect to the RNase III mutation, the DEGs in the RNA-seq data may partly result from the slow growth phenotype associated with the mutation (Fig. 1B) (Sim et al., 2010). In addition, changes in transcript abundance may be associated with various mechanisms related to RNA half-life, such as changes in translation rates and loss of RNase III-mediated cleavage events (Lee et al., 2019; Lim & Lee, 2015; Lim et al., 2012; Sim et al., 2010, 2014).

A predominant phenotype of the Δ*rnc* strain was motility loss (Fig. 4), followed by markedly decreased flagellar-associated gene expression (Figs. 1, 2). Nevertheless, in RNA-seq and qRT-PCR analyses, the *ydiV* gene, which acts as a negative regulator of FlhDC expression, showed increased expression levels in the Δ*rnc* strain (Figs. 1, 3 and Table 3). These findings indicate the importance of modulation of *ydiV* gene expression by RNase III. In fact, YdiV binds to FlhDC to shut off the transcription of secondary and tertiary flagellar genes, thereby terminating flagellum biogenesis (Wang et al., 2022). Accordingly, the increase in *ydiV* mRNA abundance likely contributed to the reduced flagellar numbers and lengths, as well as the motility loss observed in the Δ*rnc* strain. As flagellar biogenesis affects bacterial virulence by inducing motility toward the host, promoting host attachment and host cell invasion, and secreting

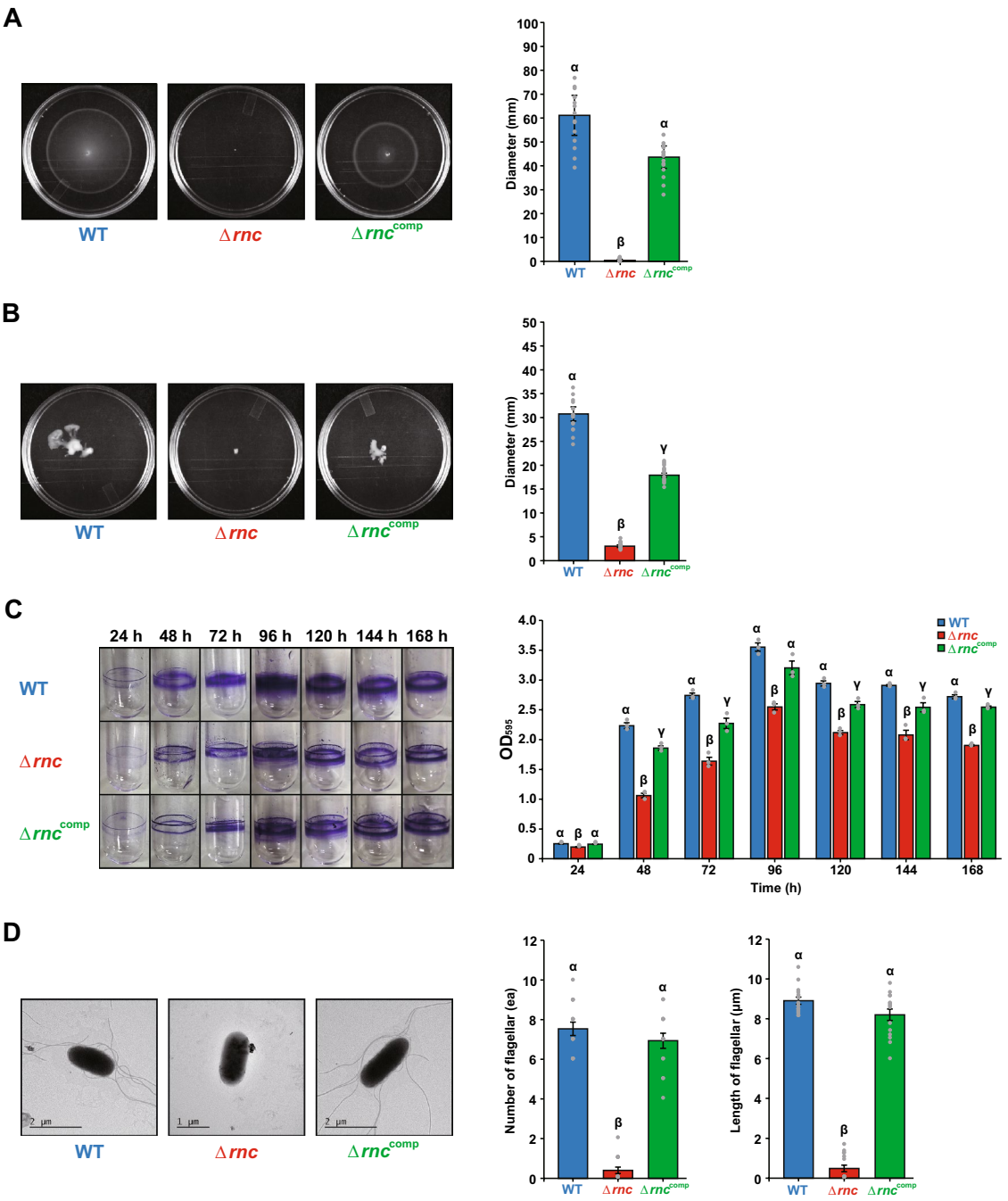

Fig. 4 Effects of RNase III levels on motility, biofilm formation, and flagellar synthesis in *S.* Typhimurium. Analysis of **A** swimming and **B** swarming motilities in WT, Δ*rnc*, and Δ*rnc*^{comp} *S.* Typhimurium strains. Swimming and swarming motilities of the cells were measured by plating them on 0.3% LB agar plates and 0.5% LB agar plates supplemented with 0.5% glucose, respectively. The experiments in (**A**) and (**B**) were conducted in five parallel runs, with three replicates each. **C** Biofilm formation in WT, Δ*rnc*, and Δ*rnc*^{comp} *S.* Typhimurium strains. Active cultures of *S.* Typhimurium strains were diluted to a final concentration of $OD_{600}=0.2$ and seeded onto borosilicate tubes containing LB medium without NaCl (LB^{-NaCl}) supplemented with ampicillin (100 μg/ml). The tubes were then incubated under static conditions at 20 °C, for 24, 48, 72, 96, 120, 144, and 168 h. The corresponding dyes were dissolved and measured using a spectrophotometer, at OD_{595}. Data were analyzed using one-way analysis of variance, with the Student–Newman–Keuls test ($p<0.0001$ for 48, 72, 120, and 168 h; $p<0.001$ for 24, 96, and 144 h). **D** Flagellar synthesis in the WT, Δ*rnc*, and Δ*rnc*^{comp} *S.* Typhimurium strains. The numbers and lengths of flagellar in the cells were measured using transmission electron microscopy images of negatively stained samples and ImageJ software (magnification: 2500×, WT and Δ*rnc*^{comp} strains; 5000×, Δ*rnc* strain). For (**A**), (**B**), and (**D**), the data were analyzed using one-way analysis of variance, with the Student–Newman–Keuls test ($p<0.0001$). For (**A**), (**B**), (**C**), and (**D**), the data represent mean ± s.e.m. of at least three independent experiments. Statistically significant differences have been indicated using distinct Greek letters. OD, optical density

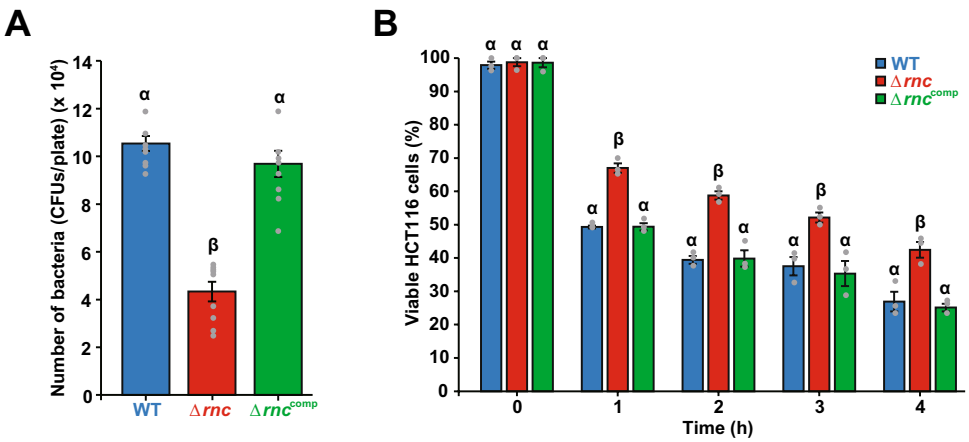

Fig. 5 Effects of RNase III levels on *S.* Typhimurium pathogenicity. **A** Effect of *rnc* expression on *S.* Typhimurium epithelial cell invasion. Human colorectal intestinal epithelial carcinoma cells (HCT116; 1×10^4 cells/well) were infected with *S.* Typhimurium strains (WT, Δ*rnc*, and Δ*rnc*^{comp}) at an MOI of 100. The number of intracellular bacteria was then quantified as CFUs. Data were analyzed using one-way ANOVA with the Student–Newman–Keuls test ($p < 0.0001$). **B** Effect of *rnc* expression on *S.* Typhimurium cell viability. HCT116 cells were infected with the *S.* Typhimurium cultures used in (**A**), at an MOI of 100. Cell viability was assessed by counting viable cells using a trypan blue staining assay at the indicated time points. Data were analyzed using one-way ANOVA, with the Student–Newman–Keuls test ($p < 0.0001$ for 1 h, $p < 0.001$ for 2 h, $p < 0.05$ for 3 h, and $p < 0.01$ for 4 h). For (**A**) and (**B**), the data represent mean ± s.e.m. of at least three independent experiments. Statistically significant differences have been indicated using distinct Greek letters. MOI, multiplicity of infection; CFU, colony-forming units

virulence factors (Haiko & Westerlund-Wikstrom, 2013), the Δ*rnc* strain phenotypes may be related to reduced host cell invadability and virulence, as compared to those of the WT and Δ*rnc*^{comp} strain phenotypes (Fig. 5). In particular, *S.* Typhimurium with the RNase III mutation exhibited attenuated virulence and proliferation in *G. mellonella* and mice (Viegas et al., 2013). However, how RNase III regulates *ydiV* gene expression remains unclear, and future studies should investigate the same via biochemical and biophysical experiments.

The cellular levels of RNase III in *E. coli* are regulated posttranscriptionally through several mechanisms. These include endoribonucleolytic cleavage of the mRNA encoding the enzyme (Bardwell et al., 1989; Matsunaga et al., 1996), upregulation through bacteriophage kinase-mediated phosphorylation (Lee et al., 2021a; Rahmsdorf et al., 1974), and protein inhibitor (YmdB)-aided down-regulation (Kim et al., 2008; Lee et al., 2021a). Pathways for regulating RNase III activity in response to osmotic changes and exposure to aminoglycoside antibiotics have been uncovered (Lim et al., 2012; Sim et al., 2010, 2014; Song et al., 2014). These results indicate the importance of modulating RNase III expression and activity in bacterial physiology. In *S.* Typhimurium, mutations in ribonucleases have been linked to alterations in pathogenicity and virulence. However, these alterations may stem from pleiotropic effects induced by these mutant ribonucleases, given that ribonuclease expression can affect the abundance of numerous mRNA species in *E. coli* (Sim et al., 2010). Homologues of RNase III are found in closely related pathogenic bacterial species, such as *Salmonella*, pathogenic *E. coli*, *Shigella dysenteriae*, *Enterobacter* sp., and *Klebsiella pneumoniae* (Fig. S1). This indicates the presence of conserved functions of RNase III in these bacterial species. Future studies should investigate whether other pathogenic bacteria have different pathogenicity regulatory pathways through RNase III-associated regulation involving flagellar assembly modulation.

In this study, we provide experimental evidence affirming the role of RNase III as a positive regulator of flagellar assembly and motility, potentially impacting *S.* Typhimurium pathogenicity. We also observed its positive effects on the abundance of mRNA species of flagellar-associated genes. Overall, this research highlights the impact of RNase III on pathogenicity-related processes in *S.* Typhimurium, underscoring the pivotal role of this well-conserved RNase III homologue in pathogenic bacteria.

Supplementary Information The online version contains supplementary material available at https://doi.org/10.1007/s12275-023-00099-5.

Acknowledgements We thank Dr. Jinsoo Kim for his technical assistance. This work was supported by the National Research Foundation of Korea (NRF) grant funded by the Korea government (Ministry of Science and ICT; MSIT) (Grant No. 2022R1F1A1070791 and RS-2023-00210754).

Data availability The raw RNA-seq data generated in this study have been deposited in the National Center for Biotechnology Information Sequence Read Archive, under the BioProject accession number PRJNA967189 (http://www.ncbi.nlm.nih.gov/sra/PRJNA967189).

Declarations

Conflict of interest The authors declare that they have no conflicts of interest.

Ethical approval All procedures involving animal studies were approved by the Institutional Animal Care and Use Committee of Hallym University (Hallym 2022-47).

References

Aldridge, P., & Hughes, K. T. (2002). Regulation of flagellar assembly. *Current Opinion in Microbiology, 5*, 160–165.

Bardwell, J. C., Regnier, P., Chen, S. M., Nakamura, Y., Grunberg-Manago, M., & Court, D. L. (1989). Autoregulation of RNase III operon by mRNA processing. *The EMBO Journal, 8*, 3401–3407.

Bechhofer, D. H., & Deutscher, M. P. (2019). Bacterial ribonucleases and their roles in RNA metabolism. *Critical Reviews in Biochemistry and Molecular Biology, 54*, 242–300.

Boisset, S., Geissmann, T., Huntzinger, E., Fechter, P., Bendridi, N., Possedko, M., Chevalier, C., Helfer, A. C., Benito, Y., Jacquier, A., & Gaspin, C. (2007). *Staphylococcus aureus* RNAIII coordinately represses the synthesis of virulence factors and the transcription regulator Rot by an antisense mechanism. *Genes & Development, 21*, 1353–1366.

Brenner, F. W., Villar, R. G., Angulo, F. J., Tauxe, R., & Swaminathan, B. (2000). *Salmonella* nomenclature. *Journal of Clinical Microbiology, 38*, 2465–2467.

Buckle, G. C., Walker, C. L., & Black, R. E. (2012). Typhoid fever and paratyphoid fever: Systematic review to estimate global morbidity and mortality for 2010. *Journal of Global Health, 2*, 010401.

Chaban, B., Hughes, H. V., & Beeby, M. (2015). The flagellum in bacterial pathogens: For motility and a whole lot more. *Seminars in Cell & Developmental Biology, 46*, 91–103.

Chang, A. C., & Cohen, S. N. (1978). Construction and characterization of amplifiable multicopy DNA cloning vehicles derived from the P15A cryptic miniplasmid. *Journal of Bacteriology, 134*, 1141–1156.

Chevance, F. F., & Hughes, K. T. (2008). Coordinating assembly of a bacterial macromolecular machine. *Nature Reviews Microbiology, 6*, 455–465.

Chilcott, G. S., & Hughes, K. T. (2000). Coupling of flagellar gene expression to flagellar assembly in *Salmonella enterica* serovar Typhimurium and *Escherichia coli*. *Microbiology and Molecular Biology Reviews, 64*, 694–708.

Deutscher, M. P. (2021). Regulation of bacterial ribonucleases. *Annual Review of Microbiology, 5*, 71–86.

Duan, Q., Zhou, M., Zhu, L., & Zhu, G. (2013). Flagella and bacterial pathogenicity. *Journal of Basic Microbiology, 53*, 1–8.

Echazarreta, M. A., & Klose, K. E. (2019). *Vibrio* flagellar synthesis. *Frontiers in Cellular and Infection Microbiology, 9*, 131.

Galán, J. E. (2021). *Salmonella* Typhimurium and inflammation: A pathogen-centric affair. *Nature Reviews Microbiology, 19*, 716–725.

Gentleman, R. C., Carey, V. J., Bates, D. M., Bolstad, B., Dettling, M., Dudoit, S., Ellis, B., Gautier, L., Ge, Y., Gentry, J., & Hornik, K. (2004). Bioconductor: Open software development for computational biology and bioinformatics. *Genome Biology, 5*, R80.

Gordon, G. C., Cameron, J. C., & Pfleger, B. F. (2017). RNA sequencing identifies new RNase III cleavage sites in *Escherichia coli* and reveals increased regulation of mRNA. *mBio, 8*, e00128-17.

Haiko, J., & Westerlund-Wikstrom, B. (2013). The role of the bacterial flagellum in adhesion and virulence. *Biology, 2*, 1242–1267.

Has, E. G., Akcelik, N., & Akcelik, M. (2023). Comparative global gene expression analysis of biofilm forms of *Salmonella* Typhimurium ATCC 14028 and its *seqA* mutant. *Gene, 853*, 147094.

Hoiseth, S. K., & Stocker, B. A. (1981). Aromatic-dependent *Salmonella* Typhimurium are non-virulent and effective as live vaccines. *Nature, 291*, 238–239.

Horstmann, J. A., Lunelli, M., Cazzola, H., Heidemann, J., Kuhne, C., Steffen, P., Szefs, S., Rossi, C., Lokareddy, R. K., Wang, C., & Lemaire, L. (2020). Methylation of *Salmonella* Typhimurium flagella promotes bacterial adhesion and host cell invasion. *Nature Communications, 11*, 2013.

Huntzinger, E., Boisset, S., Saveanu, C., Benito, Y., Geissmann, T., Namane, A., Lina, G., Etienne, J., Ehresmann, B., Ehresmann, C., & Jacquier, A. (2005). *Staphylococcus aureus* RNAIII and the endoribonuclease III coordinately regulate *spa* gene expression. *The EMBO Journal, 24*, 824–835.

Ide, N., Ikebe, T., & Kutsukake, K. (1999). Reevaluation of the promoter structure of the class 3 flagellar operons of *Escherichia coli* and *Salmonella*. *Genes & Genetic Systems, 74*, 113–116.

Josenhans, C., & Suerbaum, S. (2002). The role of motility as a virulence factor in bacteria. *International Journal of Medical Microbiology, 291*, 605–614.

Kanehisa, M., & Goto, S. (2000). KEGG: Kyoto encyclopedia of genes and genomes. *Nucleic Acids Research, 28*, 27–30.

Karlinsey, J. E., Tanaka, S., Bettenworth, V., Yamaguchi, S., Boos, W., Aizawa, S. I., & Hughes, K. T. (2000). Completion of the hook-basal body complex of the *Salmonella* Typhimurium flagellum is coupled to FlgM secretion and *fliC* transcription. *Molecular Microbiology, 37*, 1220–1231.

Kim, D., Kwon, S., Rhee, J. W., Kim, K. D., Kim, Y. E., Park, C. S., Choi, M. J., Suh, J. G., Kim, D. S., Lee, Y., & Kwon, H. J. (2011). Production of antibodies with peptide-CpG-DNA-liposome complex without carriers. *BMC Immunology, 12*, 29.

Kim, D., Lee, Y., & Kwon, H. J. (2015). Production of epitope-specific antibodies by immunization with synthetic epitope peptide formulated with CpG-DNA-liposome complex without carriers. In G. Houen (Ed.), *Peptide antibodies. Methods in molecular biology.* (Vol. 1348). New York: Humana Press.

Kim, K. S., Manasherob, R., & Cohen, S. N. (2008). YmdB: A stress-responsive ribonuclease-binding regulator of *E. coli* RNase III activity. *Genes & Development, 22*, 3497–3508.

Kutsukake, K., Ohya, Y., & Iino, T. (1990). Transcriptional analysis of the flagellar regulon of *Salmonella* Typhimurium. *Journal of Bacteriology, 172*, 741–747.

Lee, J., Lee, M., & Lee, K. (2021a). *Trans*-acting regulators of ribonuclease activity. *Journal of Microbiology, 59*, 341–359.

Lee, J., Shin, E., Park, J., Lee, M., & Lee, K. (2021b). Regulator of ribonuclease activity modulates the pathogenicity of *Vibrio vulnificus*. *Journal of Microbiology, 59*, 1133–1141.

Lee, J., Shin, E., Yeom, J. H., Park, J., Kim, S., Lee, M., & Lee, K. (2022). Regulator of RNase E activity modulates the pathogenicity of *Salmonella* Typhimurium. *Microbial Pathogenesis, 165*, 105460.

Lee, M., Joo, M., Sim, M., Sim, S. H., Kim, H. L., Lee, J., Ryu, M., Yeom, J. H., Hahn, Y., Ha, N. C., & Cho, J. C. (2019). The coordinated action of RNase III and RNase G controls enolase expression in response to oxygen availability in *Escherichia coli*. *Scientific Reports, 9*, 17257.

Lee, M., Ryu, M., Joo, M., Seo, Y. J., Lee, J., Kim, H. M., Shin, E., Yeom, J. H., Kim, Y. H., Bae, J., & Lee, K. (2021c). Endoribonuclease-mediated control of *hns* mRNA stability constitutes a key regulatory pathway for *Salmonella* Typhimurium pathogenicity island 1 expression. *PLoS Pathogens, 17*, e1009263.

Lim, B., & Lee, K. (2015). Stability of the osmoregulated promoter-derived *proP* mRNA is posttranscriptionally regulated by RNase III in *Escherichia coli*. *Journal of Bacteriology, 197*, 1297–1305.

Lim, B., Sim, M., Lee, H., Hyun, S., Lee, Y., Hahn, Y., Shin, E., & Lee, K. (2015). Regulation of *Escherichia coli* RNase III activity. *Journal of Microbiology, 53*, 487–494.

Lim, B., Sim, S. H., Sim, M., Kim, K., Jeon, C. O., Lee, Y., Ha, N. C., & Lee, K. (2012). RNase III controls the degradation of *corA* mRNA in *Escherichia coli*. *Journal of Bacteriology, 194*, 2214–2220.

Majowicz, S. E., Musto, J., Scallan, E., Angulo, F. J., Kirk, M., O'Brien, S. J., Jones, T. F., Fazil, A., Hoekstra, R. M., for the International Collaboration on Enteric Disease 'Burden of Illness Studies. (2010). The global burden of nontyphoidal *Salmonella* gastroenteritis. *Clinical Infectious Diseases, 50*, 882–889.

Matsunaga, J., Simons, E. L., & Simons, R. W. (1996). RNase III autoregulation: Structure and function of *rncO*, the posttranscriptional "operator." *RNA, 2*, 1228–1240.

Miao, E. A., Leaf, I. A., Treuting, P. M., Mao, D. P., Dors, M., Sarkar, A., Warren, S. E., Wewers, M. D., & Aderem, A. (2010). Caspase-1-induced pyroptosis is an innate immune effector mechanism against intracellular bacteria. *Nature Immunology, 11*, 1136–1142.

Minamino, T., Morimoto, Y. V., Kinoshita, M., & Namba, K. (2021). Multiple roles of flagellar export chaperones for efficient and robust flagellar filament formation in *Salmonella*. *Frontiers in Microbiology, 12*, 756044.

Moffatt, C. R. M., Musto, J., Pingault, N., Miller, M., Stafford, R., Gregory, J., Polkinghorne, B. G., & Kirk, M. D. (2016). *Salmonella* Typhimurium and outbreaks of egg-associated disease in Australia, 2001 to 2011. *Foodborne Pathogens and Disease, 13*, 379–385.

Mohanty, B. K., & Kushner, S. R. (2018). Enzymes involved in post-transcriptional RNA metabolism in gram-negative bacteria. *Microbiol Spectrum*. https://doi.org/10.1128/microbiolspec.rwr-0011-2017

Morimoto, Y. V., & Minamino, T. (2021). Architecture and assembly of the bacterial flagellar motor complex. In J. R. Harris & J. Marles-Wright (Eds.), *Macromolecular protein complexes III: Structure and function. Subcellular biochemistry.* (Vol. 96). Springer.

Na, D. (2020). User guides for biologists to learn computational methods. *Journal of Microbiology, 58*, 173–175.

Okada, Y., Wachi, M., Hirata, A., Suzuki, K., Nagai, K., & Matsuhashi, M. (1994). Cytoplasmic axial filaments in *Escherichia coli* cells: Possible function in the mechanism of chromosome segregation and cell division. *Journal of Bacteriology, 176*, 917–922.

Pati, N. B., Vishwakarma, V., Jaiswal, S., Periaswamy, B., Hardt, W. D., & Suar, M. (2013). Deletion of *invH* gene in *Salmonella enterica* serovar Typhimurium limits the secretion of Sip effector proteins. *Microbes and Infection, 15*, 66–73.

Popoff, M. Y., Bockemühl, J., & Brenner, F. W. (2000). Supplement 1998 (no. 42) to the Kauffmann-White scheme. *Research in Microbiology, 151*, 63–65.

Raffatellu, M., Wilson, R. P., Chessa, D., Andrews-Polymenis, H., Tran, Q. T., Lawhon, S., Khare, S., Adams, L. G., & Baumler, A. J. (2005). SipA, SopA, SopB, SopD, and SopE2 contribute to *Salmonella enterica* serotype Typhimurium invasion of epithelial cells. *Infection and Immunity, 73*, 146–154.

Rahmsdorf, H. J., Pai, S. H., Ponta, H., Herrlich, P., Roskoski, R., Jr., Schweiger, M., & Studier, F. W. (1974). Protein kinase induction in *Escherichia coli* by bacteriophage T7. *Proceedings of the National Academy of Sciences of the United States of America, 71*, 586–589.

Sim, M., Lim, B., Sim, S. H., Kim, D., Jung, E., Lee, Y., & Lee, K. (2014). Two tandem RNase III cleavage sites determine *betT* mRNA stability in response to osmotic stress in *Escherichia coli*. *PLoS ONE, 9*, e100520.

Sim, S. H., Yeom, J. H., Shin, C., Song, W. S., Shin, E., Kim, H. M., Cha, C. J., Han, S. H., Ha, N. C., Kim, S. W., & Hahn, Y. (2010). *Escherichia coli* ribonuclease III activity is downregulated by osmotic stress: Consequences for the degradation of *bdm* mRNA in biofilm formation. *Molecular Microbiology, 75*, 413–425.

Smith, S. I., Seriki, A., & Ajayi, A. (2016). Typhoidal and non-typhoidal *Salmonella* infections in Africa. *European Journal of Clinical Microbiology & Infectious Diseases, 35*, 1913–1922.

Song, W., Joo, M., Yeom, J. H., Shin, E., Lee, M., Choi, H. K., Hwang, J., Kim, Y. I., Seo, R., Lee, J. E., & Moore, C. J. (2019). Divergent rRNAs as regulators of gene expression at the ribosome level. *Nature Microbiology, 4*, 515–526.

Song, W., Kim, Y. H., Sim, S. H., Hwang, S., Lee, J. H., Lee, Y., Bae, J., Hwang, J., & Lee, K. (2014). Antibiotic stress-induced modulation of the endoribonucleolytic activity of RNase III and RNase G confers resistance to aminoglycoside antibiotics in *Escherichia coli*. *Nucleic Acids Research, 42*, 4669–4681.

Stecher, B., Hapfelmeier, S., Müller, C., Kremer, M., Stallmach, T., & Hardt, W. D. (2004). Flagella and chemotaxis are required for efficient induction of *Salmonella enterica* serovar Typhimurium colitis in streptomycin-pretreated mice. *Infection and Immunity, 72*, 4138–4150.

Stecher, B., Robbiani, R., Walker, A. W., Westendorf, A. M., Barthel, M., Kremer, M., Chaffron, S., Macpherson, A. J., Buer, J., Parkhill, J., & Dougan, G. (2007). *Salmonella enterica* serovar Typhimurium exploits inflammation to compete with the intestinal microbiota. *PLoS Biology, 5*, 2177–2189.

Stewart, M. K., Cummings, L. A., Johnson, M. L., Berezow, A. B., & Cookson, B. T. (2011). Regulation of phenotypic heterogeneity permits *Salmonella* evasion of the host caspase-1 inflammatory response. *Proceedings of the National Academy of Sciences of the United States of America, 108*, 20742–20747.

Svensson, S. L., & Sharma, C. M. (2021). RNase III-mediated processing of a *trans*-acting bacterial sRNA and its *cis*-encoded antagonist. *eLife, 10*, e69064.

Szklarczyk, D., Gable, A. L., Lyon, D., Junge, A., Wyder, S., Huerta-Cepas, J., Simonovic, M., Doncheva, N. T., Morris, J. H., Bork, P., & Jensen, L. J. (2019). STRING v11: Protein-protein association networks with increased coverage, supporting functional discovery in genome-wide experimental datasets. *Nucleic Acids Research, 47*, D607–D613.

The UniProt Consortium. (2018). UniProt: The universal protein knowledgebase. *Nucleic Acids Research, 46*, 2699.

Thomason, M. K., Bischler, T., Eisenbart, S. K., Förstner, K. U., Zhang, A., Herbig, A., Nieselt, K., Sharma, C. M., & Storz, G. (2015). Global transcriptional start site mapping using differential RNA sequencing reveals novel antisense RNAs in *Escherichia coli*. *Journal of Bacteriology, 197*, 18–28.

Tomoyasu, T., Takaya, A., Isogai, E., & Yamamoto, T. (2003). Turnover of FlhD and FlhC, master regulator proteins for *Salmonella* flagellum biogenesis, by the ATP-dependent ClpXP protease. *Molecular Microbiology, 48*, 443–452.

Viegas, S. C., Mil-Homens, D., Fialho, A. M., & Arraiano, C. M. (2013). The virulence of *Salmonella enterica* Serovar Typhimurium in the insect model *Galleria mellonella* is impaired by mutations in RNase E and RNase III. *Applied and Environmental Microbiology, 79*, 6124–6133.

Wang, S., Fleming, R. T., Westbrook, E. M., Matsumura, P., & McKay, D. B. (2006). Structure of the *Escherichia coli* FlhDC complex, a prokaryotic heteromeric regulator of transcription. *Journal of Molecular Biology, 355*, 798–808.

Wang, W., Yue, Y., Zhang, M., Song, N., Jia, H., Dai, Y., Zhang, F., Li, C., & Li, B. (2022). Host acid signal controls *Salmonella* flagella biogenesis through CadC-YdiV axis. *Gut Microbes, 14*, 2146979.

Yanagihara, S., Iyoda, S., Ohnishi, K., Iino, T., & Kutsukake, K. (1999). Structure and transcriptional control of the flagellar master operon of *Salmonella* Typhimurium. *Genes & Genetic Systems, 74*, 105–111.

Yokoyama, W. M., Christensen, M., Santos, G. D., & Miller, D. (2006). Production of monoclonal antibodies. *Current Protocols in Immunology, 2*, 251–252.

Yue, Y., Wang, W., Ma, Y., Song, N., Jia, H., Li, C., Wang, Q., Li, H., & Li, B. (2023). Cooperative regulation of flagellar synthesis by two EAL-like proteins upon *Salmonella* entry into host cells. *Microbiol Spectrum, 11*, e02859–22.